JACS
JOURNAL OF THE AMERICAN CHEMICAL SOCIETY
Article
Cite This: J. Am. Chem. Soc. 2018, 140, 14308−14313
pubs.acs.org/JACS

Effect of Structure on the Spin−Spin Interactions of Tethered Dicyanomethyl Diradicals

Rui Zhang,[†] Joshua P. Peterson,[†] Logan J. Fischer, Arkady Ellern, and Arthur H. Winter*

Department of Chemistry, Iowa State University, 1608 Gilman Hall, Ames, Iowa 50010, United States

Supporting Information

ABSTRACT: Stable organic radicals with switchable spin states have attracted attention for a variety of applications, but a fundamental understanding of how radical structure effects the weak bonding interactions between organic radicals is limited. To evaluate the effect of chemical structure on the strength and nature of such spin interactions, a series of 14 tethered aryl dicyanomethyl diradicals were synthesized, and the structure and thermodynamic properties of the diradicals were investigated. These studies indicate that the nature of the dimer and the equilibrium thermodynamic parameters of the diradical−dimer equilibria are highly sensitive to the attachment point of the linker, the length of the linker, and the substituents on the radical itself. Values of the intramolecular K_a vary from as small as 5 to as high as 10^5 depending on these variables. An X-ray crystal structure for a linked *ortho*-substituted diradical shows that the diradical forms an intramolecular sigma dimer in the crystalline state with an elongated C−C bond (1.637 Å). Subtle changes to the radical structure influences the nature of the spin interactions, as fixing the dimethylamino substituent on the radical into a ring to make a julolidine-derived diradical leads to the weakest bonding interaction observed ($\Delta G_{bonding}$ = 1 kcal mol^{-1}) and changes the spin-paired species from a sigma dimer to a diradical pimer. This work has implications for the design of stimuli-responsive materials that can reversibly switch between the dramatically different properties of closed-shell species and the unique properties of diradicals.

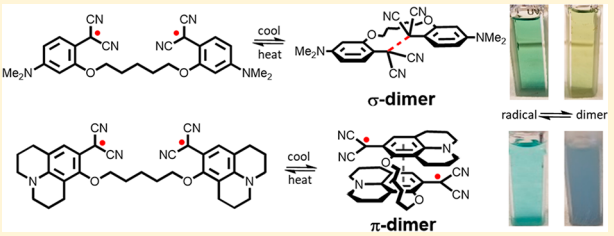

INTRODUCTION

The ability of open-shell species to form weak self-association complexes has made organic radicals attractive for a variety of applications including organic spin-crossover materials,[1] turn-on magnetic resonance contrast reagents,[2] stimuli-responsive soft materials,[3] spintronics,[4] and dynamic covalent assemblies derived from stable radical building blocks.[5] However, a fundamental understanding of how radical structure affects the weak bonding interactions between organic radicals is limited by the scarcity of radicals that engage in this behavior with sufficient stability for detailed study.

Aryl dicyanomethyl radicals make attractive candidates for such studies.[6] These radicals, and related species, have been known for many years to persist long enough to collect electron paramagnetic resonance (EPR) spectra, but were long overlooked for applications because they undergo an irreversible "head-to-tail" dimerization[6] that destroys the radical. However, in 2016 Seki and co-workers demonstrated that these radicals become indefinitely air and thermally stable species provided that *para* substituents are added to block this dead-end head-to-tail dimerization pathway.[6] Normally, to achieve air stability, organic radicals must be substituted with sterically blocking groups near the radical center.[7] That these aryl dicyanomethyl radicals do not require such sterically blocking groups for stability is unusual and permits these stable radicals to form weak-bonding spin−spin interactions in solution as diamagnetic dimers, straddling the knife-edge between normal closed-shell molecules and stable diradicals in both structure and properties. As a result, they are intriguing building blocks for stimuli-responsive materials that can switch between the dramatically different properties of closed-shell species and the unique properties of diradicals.

Following Seki's discovery, we performed structure−activity relationships on aryl dicyanomethyl monoradicals and found that electron-donating groups appended to the aryl ring shift the equilibrium toward the diradical,[8] while withdrawing groups shift the equilibrium toward diamagnetic dimers. With *para* substituents, the bond strength is correlated with the Hammett σ_{para} substituent parameter. Thus, the radical−radical interaction can be tuned by substituents. However, whether these radicals can be used in larger structures featuring multiple radical centers remains unknown. A key problem in achieving this objective is understanding how the radicals interact when covalently linked.

Here we report a detailed study of the effect of chemical structure on the strength and nature of the spin−spin interactions for linked aryl dicyanomethyl diradicals. A series of 14 tethered aryl dicyanomethyl diradicals were synthesized (Figure 1), and the thermodynamic bonding parameters were elucidated using variable-temperature EPR and UV−vis spectroscopy, X-ray crystallography, and computational anal-

Received: August 11, 2018
Published: October 2, 2018

DOI: 10.1021/jacs.8b08628
J. Am. Chem. Soc. 2018, 140, 14308−14313

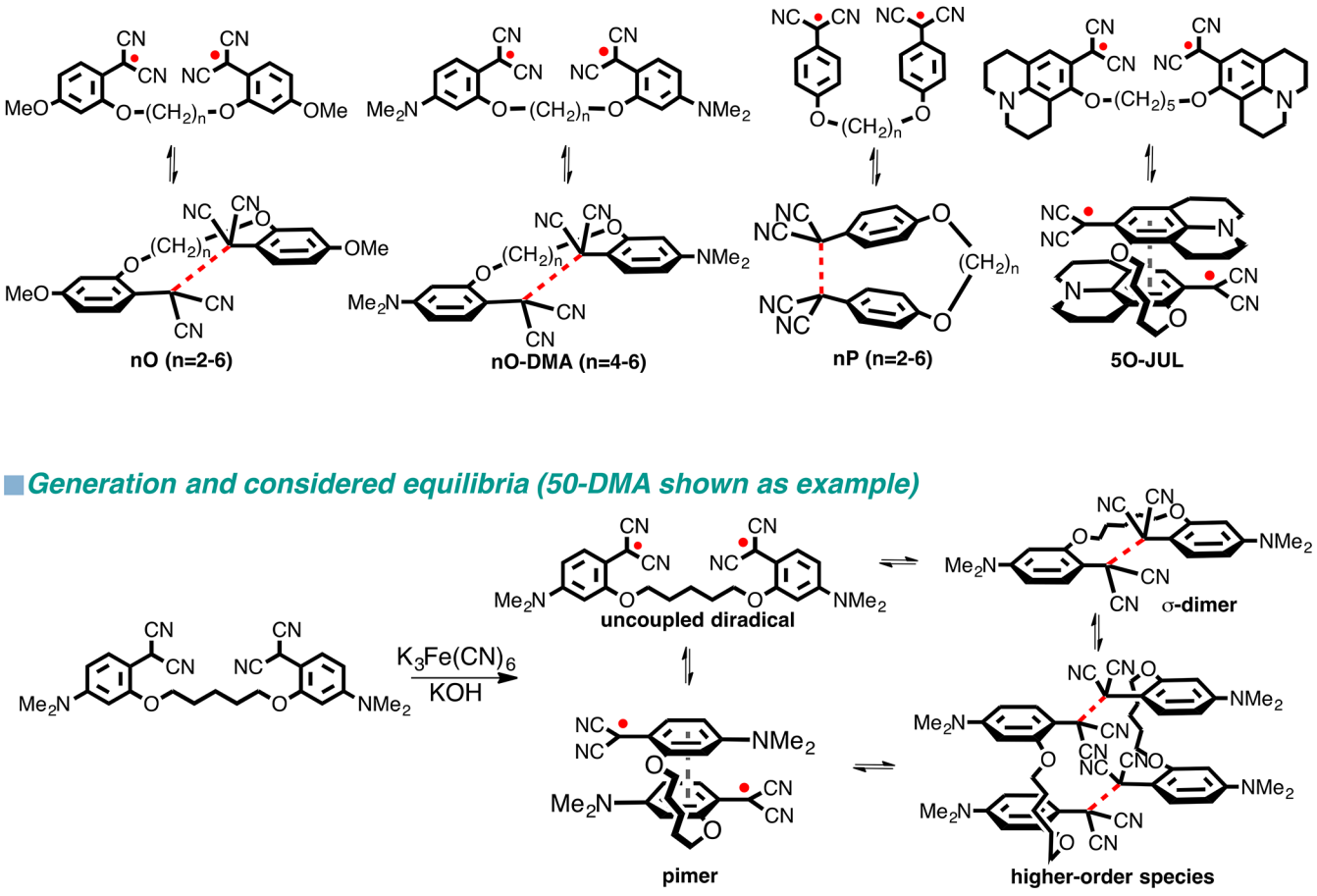

Figure 1. (Top) The 14 linked diradicals synthesized and studied in this paper. (Bottom) Generation and considered equilibria for diradicals.

ysis (Table 1). We find that the strength of the intramolecular spin−spin interaction is exquisitely sensitive to the structure of the radical, the substitution position of the linker, and the length of the linker, with the association constant varying over 5 orders of magnitude by changing these variables. Subtle changes to the radical structure are found to alter the nature of the spin−spin interaction, as a *p*-dimethylamino-substituted tethered diradical **5O-DMA** forms a sigma dimer with an elongated bond, while a structurally related julolidine derivative **5O-JUL** forms an exceedingly weakly bonded pimer ($\Delta G_{bonding}$ = 1 kcal/mol). Furthermore, a serendipitously discovered photochemical coupling reaction allows the radicals to be irreversibly locked upon irradiation via formation of a long-wavelength-absorbing rhodamine dye derivative (λ_{max} ≈ 725 nm) and formal loss of a dicyanomethyl group, providing a potentially useful tool for both irreversibly phototrapping metastable dynamic covalent assemblies and providing an optical readout. Overall, this work shows how structural changes can be used to control the strength and nature of intramolecular spin−spin interactions, which has implications for dynamic covalent assemblies and stimuli-responsive polymers using this new class of stable diradicals as building blocks.

RESULTS AND DISCUSSION

Determination of Equilibrium Species. The diradicals shown in Figure 1 were generated by quantitative oxidation of malononitrile-substituted arenes with potassium ferricyanide and the diradical purified from the inorganic byproducts by partitioning between water and dichloromethane.

Prior to any quantitative measurements, we needed to identify the species present in the equilibrium with the diradicals. Four different equilibrium species shown in Figure 1 were considered: the free diradical, a sigma dimer, a pi dimer (pimer), and higher-order aggregates. (See Figure 1, bottom.)

To evaluate whether higher-order aggregates are formed, the spin concentration as a function of diradical concentration was plotted for representative radicals **5O**, **5P**, and **6O-DMA**, at concentrations ranging from 50 μM to 10 mM. The spin concentrations were determined by double integration of the radical EPR signal. In all three cases, a linear plot was observed, indicating that the percent radical is independent of concentration, which is not consistent with the formation of higher-order diamagnetic species (see Figure SI-63). Intermolecular dimerization would be concentration dependent and would be expected to lead to a curved binding isotherm similar to what we observed for the intermolecular dimerization of the monoradicals.[8] Thus, while higher-order species may be contributors to the equilibrium at higher concentrations than those studied, they are not expected to be relevant species to the equilibria at the concentrations used here.

Next, we considered whether the diradicals were forming sigma or pi dimers. Both are possible modes of dimerization for stabilized free radicals. While both sigma and pi dimers are diamagnetic and EPR silent, sigma dimers break the conjugation of the radical and are generally colorless (or

DOI: 10.1021/jacs.8b08628
J. Am. Chem. Soc. 2018, 140, 14308−14313

Table 1. Thermodynamic Parameters for *o*-Linked (a), *p*-Linked (b), and Julolidine (c)

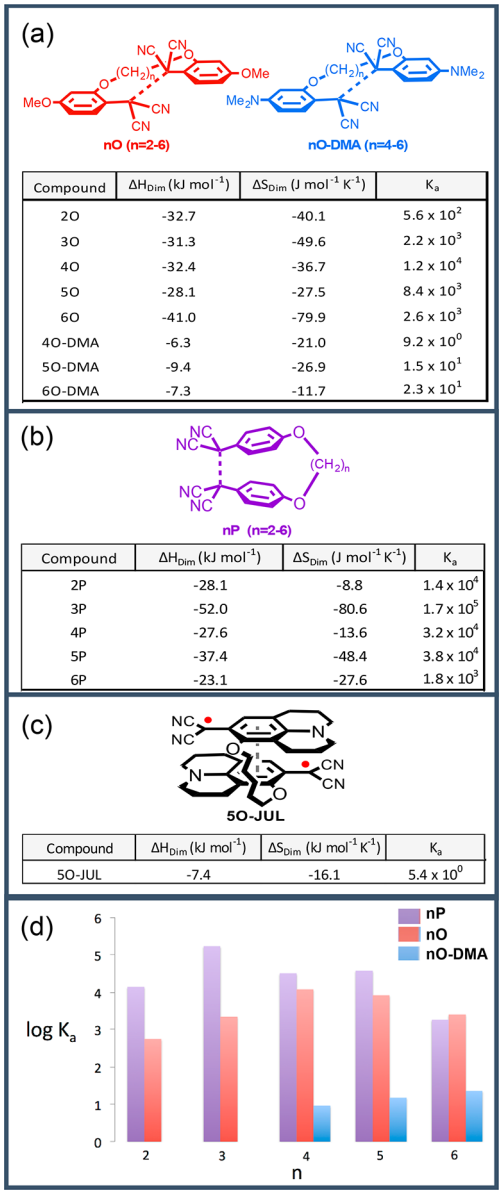

Compound	ΔH_{Dim} (kJ mol^{-1})	ΔS_{Dim} (J mol^{-1} K^{-1})	K_a
2O	-32.7	-40.1	5.6×10^2
3O	-31.3	-49.6	2.2×10^3
4O	-32.4	-36.7	1.2×10^4
5O	-28.1	-27.5	8.4×10^3
6O	-41.0	-79.9	2.6×10^3
4O-DMA	-6.3	-21.0	9.2×10^0
5O-DMA	-9.4	-26.9	1.5×10^1
6O-DMA	-7.3	-11.7	2.3×10^1

Compound	ΔH_{Dim} (kJ mol^{-1})	ΔS_{Dim} (J mol^{-1} K^{-1})	K_a
2P	-28.1	-8.8	1.4×10^4
3P	-52.0	-80.6	1.7×10^5
4P	-27.6	-13.6	3.2×10^4
5P	-37.4	-48.4	3.8×10^4
6P	-23.1	-27.6	1.8×10^3

Compound	ΔH_{Dim} (kJ mol^{-1})	ΔS_{Dim} (kJ mol^{-1} K^{-1})	K_a
5O-JUL	-7.4	-16.1	5.4×10^0

slightly yellow), whereas pimers feature near-IR absorption bands and are often colored species. Diradicals **2-6O**, **4-6O-DMA**, and **2-6P** have qualitatively the same behavior. At low temperatures, the solutions are colorless or faintly colored, while upon heating the solutions turn brightly colored and are accompanied by the growth of an EPR signal (Figure 2 shows representative photos from each class of diradical) and a UV–vis band corresponding to the diradical. This heating/cooling can be reversibly switched. This temperature-responsive behavior is consistent with an enthalpically favored sigma dimer in equilibrium with an entropically favored diradical.

In contrast, **5O-JUL** has qualitatively different behavior. At room temperature the solution is aqua-colored, which becomes darker blue upon cooling with a growth of a near-IR band >900 nm (Figure 3). As the temperature is decreased, the EPR signal also decreases and the UV–vis band associated with the diradical decreases. This behavior is consistent with an enthalpically favored diamagnetic diradical pimer existing in equilibrium with an entropically favored diradical and is also consistent with what Seki and co-workers observed for the monoradical.[6] Computational modeling of the pimer is described below. Thermal population of a sigma dimer cannot be ruled out, as the sigma dimer is not visible by EPR or UV–vis spectroscopy. From a practical point of view, the thermodynamic parameters determined in Table 1 for this species can be viewed as the EPR-active diradical–EPR-inactive diamagnetic dimer equilibrium thermodynamic parameters, with the diamagnetic dimer species possibly consisting of a Boltzmann population of at least the diamagnetic pimer and possibly the diamagnetic sigma dimer.

Effect of Linker Attachment Position and Length on the Spin–Spin Interaction Thermodynamics and Equilibria. Having established the nature of the equilibrium species, we next evaluated the effect of changing the linker size for three different substituted radicals (with differing *para* substituents) and two different linker attachment positions, at the *ortho* (**2-6O**) and *para* position (**2-6P**) to the radical center. We determined the thermodynamic intramolecular dimerization parameters (ΔG^o, ΔH^o, ΔS^o, K_a) for these diradicals from van 't Hoff plots measuring spin concentration determined by EPR spectroscopy (double integration) as a function of temperature (see SI-60). See Table 1.

Several conclusions can be made from the thermodynamic data. First, attachment position matters. In general, *ortho*-linked diradicals feature lower association constants for dimerization than the *para*-linked diradicals. For example, **3O** has a weaker binding constant than **3P** by nearly 2 orders of magnitude ($K_a = 2.2 \times 10^3$ vs 1.7×10^5, respectively). This can be attributed to strains experienced by the *ortho*-linked species with an insufficiently long linker. Second, longer linkers generally favor the diradical, leading to lower association constants. The exception is that shorter linkers with two or three carbons for the *ortho*-linked (**2-6O** diradicals) and two carbons in the case of the *para*-linked (**2-6P** diradicals) have weaker binding constants. This can be attributable to the macrocyclic ring strains encountered with an insufficiently long linker. The four-carbon linker for the *ortho*-substituted diradical and the three-carbon linker for the *para*-substituted diradical feature the largest association constants, suggesting that these tethers represent the "ideal" linker size for a trade-off between added ring strain (in the case of a short linker) and entropic penalty of binding (in the case of a longer alkyl linker). Interestingly, there is an alternating "even–odd" effect of linker size on the ΔH^o in the **2-6O** series, with all even numbers of carbons in the linker having more negative ΔH^o values than odd linker numbers. This even–odd effect does not manifest itself in the K_a values, however, as a likely result of entropy–enthalpy compensation attenuation and other effects being larger. In the *para* series **2-6P**, it is the odd number of carbons that always has a lower ΔH^o. A similar even–odd effect has been seen in the case of linked viologen cation radicals.[10] In the cases of the **4-6O-DMA** series, featuring a stronger donating dimethylamino group in the *para* position, these diradicals all feature similarly extremely weak bonding interactions (e.g., $\Delta G^o_{bonding} < 2$ kcal/mol), making trends difficult to discern. A striking result of this study is that changing the *para*-methoxy group to a *para*-dimethylamino group leads to a smaller K_a by 3–4 orders of magnitude.

Only one julolidine derivative (**5O-JUL**) was synthesized due to synthetic difficulties of making the diradical precursors. Briefly, the palladium-catalyzed cross-coupling of the diaryl

DOI: 10.1021/jacs.8b08628
J. Am. Chem. Soc. 2018, 140, 14308–14313

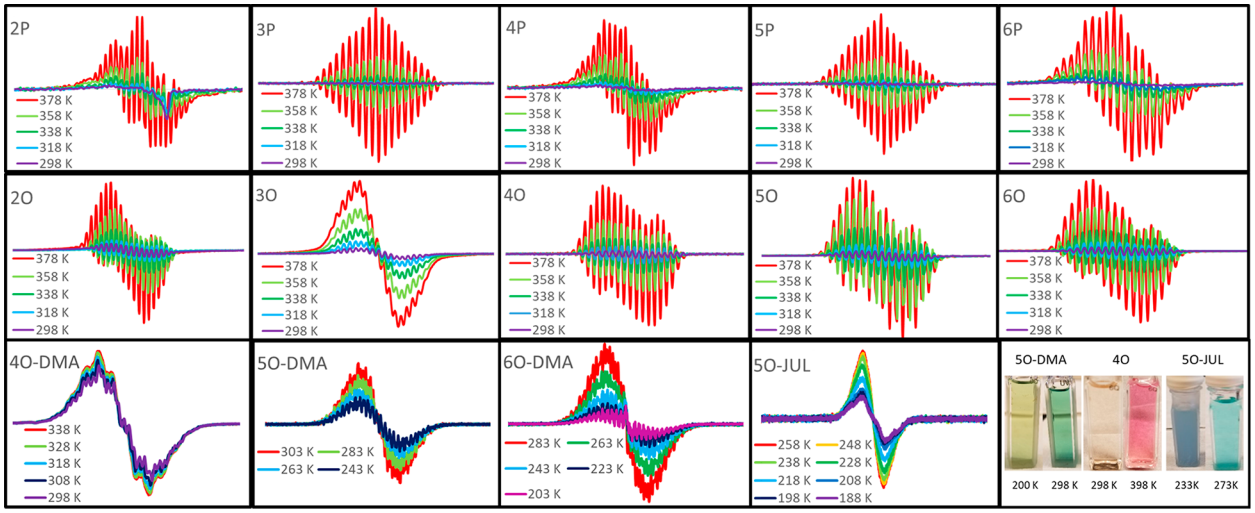

Figure 2. Electron paramagnetic resonance spectra of the diradical species of each compound with variable-temperature stimulation to study thermodynamic parameters.

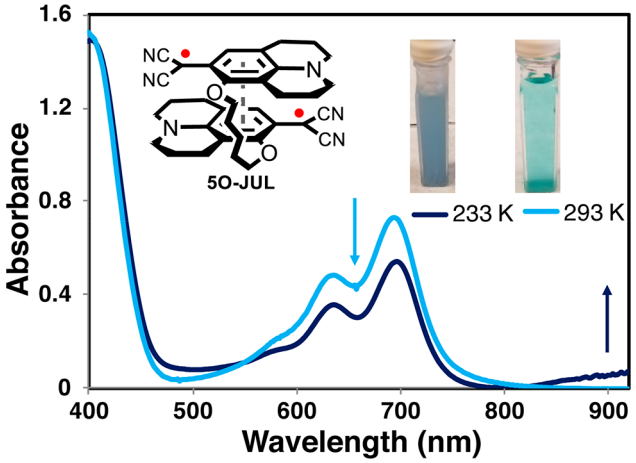

Figure 3. UV/vis spectroscopy showing the color change of compound **5O-JUL** as it cools, signifying the formation of a pimer band by the peak growing in from 850 nm.

dibromide is poisoned by the extremely electron-rich tethered diaryl substrate, leading to mostly reduction of Br to H rather than substitution with malononitrile. The julolidine is a more electron-donating substituent than dimethylamino because it locks the nitrogen into a planar conformation, forcing conjugation with the pi system of the arene.

This julolidine-derived diradical features the weakest spin–spin interaction ($\Delta G^{\circ}_{bonding}$ = 1 kcal/mol) of the series, showing that more electron-donating substituents shift the equilibrium toward the diradical (OMe ≪ NMe_2 < julolidine). As described above, the nature of the spin–spin bonding interaction also switches from an elongated sigma dimer to a pi dimer (pimer).

Computational Studies of the Nature of the Radical–Radical Interaction. To gain insight into the nature of the bonding interaction between the radicals, we turned to computational analysis. First, we sought to identify a computational method capable of handling such diradical interactions. To do this, we screened a variety of density functionals to see if any could reproduce our previously published[8] intermolecular binding free energies of the fluoro-substituted aryl dicyanomethyl monoradical (Figure 4C). Functionals lacking dispersion corrections give nonsensical predictions of the binding free energy, predicting it to be unfavorable and underestimating it by 5–25 kcal/mol. The Head-Gordon functional, ωB97XD/6-31+G(d,p), which includes a dispersion correction, was found to best reproduce the binding energy of this radical to within 3 kcal/mol. We then evaluated this level of theory against six different substituted monoradicals, for which we have previously determined experimental intermolecular binding free energies[8] and span a range of binding enthalpies (24.6 kcal mol^{-1} for Cl to 12.7 kcal mol^{-1} for NMe_2). The RMSD error for the six radicals was <2 kcal mol^{-1}, with the fluoro being the poorest predicted. The reasonable prediction of the binding free energies using this level of theory gives us confidence in using this method to evaluate new radicals, as yet unsynthesized.

Regrettably, this method erroneously predicts the sigma dimer of **5O-JUL** to be lower in energy than the pimer by 6.5 kcal/mol. In contrast, B97D/6-31+G(d,p), which gave good predictions of the pimerization of the viologen cation radical,[9] predicts the pimer to be more stable than the sigma dimer by 4.5 kcal/mol. Thus, while ωB97XD appears to accurately describe the diradical–sigma dimer bonding thermodynamics, it fails for describing the sigma-dimer–pimer equilibrium. A computationally feasible method that can accurately handle the sigma dimer–pimer equilibrium is currently being investigated.

Radical Stability and Photochemical Reactivity. In general, the diradicals described in this study feature remarkable air and thermal stability. For example, solutions of **2-6O** and **2-6P** were stable for at least 12 months. Heat/cool cycles can be performed multiple times without decomposition with two exceptions. Compounds **4-6O-DMA** and **5O-JUL** derivatives show some thermal instability at high temperature (above 60 and 40 °C, respectively).

We serendipitously discovered a photoreaction of the amino-containing diradicals. Holding up tubes of the colored diradicals to bright sunshine led to a rapid color change and irreversible loss of all EPR signal. UV–vis experiments show the formation of a species with a $\lambda_{max} \approx 725$ nm, a remarkably red-shifted absorption for a diamagnetic closed-shell species. Mass spectroscopy and NMR data are consistent with a xanthene dye-like structure corresponding to loss of a dicyanomethyl group, leading us to propose the structure

DOI: 10.1021/jacs.8b08628
J. Am. Chem. Soc. 2018, 140, 14308–14313

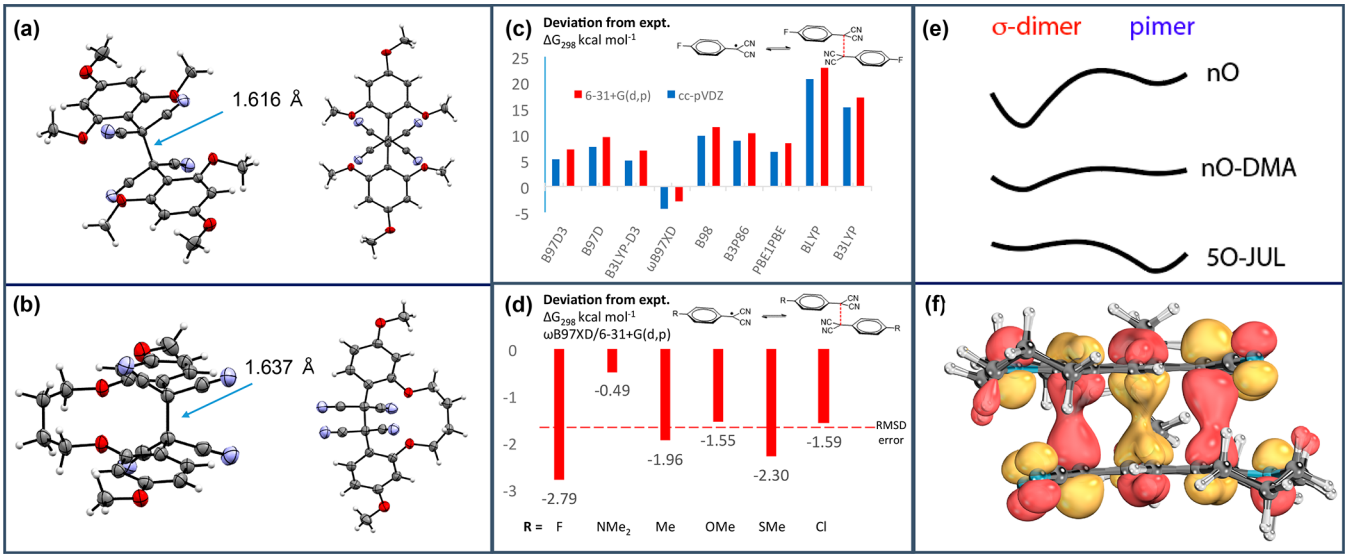

Figure 4. (a) Crystal structures for 2,4,6-trimethoxy untethered diradical dimer and (b) **4O**. (c) Computational screen of density functionals for accuracy in modeling *p*-fluorophenyl dicyanomethyl radical dimerization free energy. (d) Using the ωB97XD method to evaluate accuracy of dimerization thermodynamics over a small test set. (e) Suggested qualitative σ-dimer−pimer PES for varying substituents. (f) HOMO of julolidine pimer showing pi overlap.

shown in Figure 5, a derivative of the long-wavelength absorbing rhodamine dye (see SI for spectra). Growth of

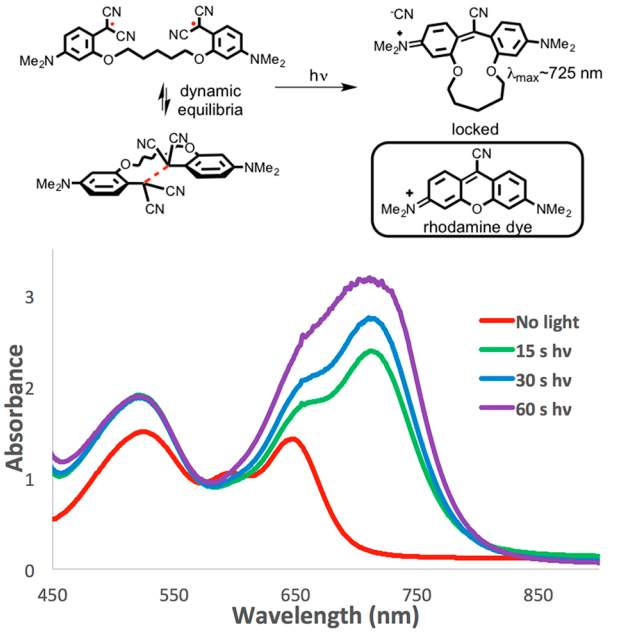

Figure 5. (Top) Amino-substituted diradical photochemistry that transforms the diradical into a rhodamine dye derivative. (Bottom) UV−vis at different times of irradiation (Rayonet, 5 × 10^{-5} M in toluene).

this absorption band occurs only for the amino derivatives. This photoreaction could prove to be useful for photochemically locking metastable dynamic covalent chemistry intermediates derived from these radicals in a way that can be monitored optically following the growth of the 725 nm absorption band.

MATERIALS AND METHODS

Variable-Temperature EPR Experiments and van't Hoff Plots. Variable-temperature EPR studies were performed on all diradicals to elucidate the bonding thermodynamic parameters for each diradical/dimer equilibria. All diradicals were investigated in toluene solvent with concentrations ranging from 1 to 5 mM, with the exception of compounds **5-6O-DMA**, requiring dichloromethane as solvent. During the EPR experiments, measurements were made using temperature increments of 10 K after allowing the sample to equilibrate for 5 min at each temperature from 298 to 378 K. A follow-up EPR scan was performed after increasing the temperature to ensure that no decomposition occurred. Diradicals **4-6O-DMA** and **5O-JUL** all showed signs of decomposition at elevated temperatures and in light. In the case of the more electron-donating compounds (**4-6O-DMA** and **5O-JUL**), EPR experiments were performed by lowering the temperature to as low as 188 K and then slowly raising the temperature up to 278 K to calculate thermodynamic parameters.

For each sample studied, toluene or dichloromethane was added to the solid sample to make a 1−5 mM solution of radical/dimer species. This solution was then purged and cannulated into a prepurged quartz EPR tube. EPR studies were then performed at 10-degree increments (298−378 K for toluene and 208−298 K for dichloromethane) with an equilibration time of 5 min for each temperature increment. The following instrument parameters were generally followed for each sample: modulation frequency, 100 kHz; receiver gain, 50 dB; modulation amplitude, 0.5; time constant, 0.01 s; center field, 3330 G; sweep width, ∼200 G; microwave attenuation, 20 dB; microwave power, 2 mW; number of data points, 2048; average number of scans, 15.

UV−Vis Spectrum for 5O-JUL. A 50 μM solution of **5O-JUL** in toluene was carefully prepared to avoid any light, air, or other contamination to detect the presence of a pimer band growing in the near-IR region as the temperature was lowered to 233 K. Low-temperature spectra were made possible by a liquid nitrogen cooler with a nitrogen blow off to avoid condensation on the quartz cell walls.

Computational Methods. All computations were carried out in Gaussian16.[11] Nontethered dimers and radicals for the computational benchmark were optimized using multiple theoretical methods, BLYP,[12] B3LYP,[13] PBE1PBE,[14] B3P86,[15] B98,[16] ωB98XD,[17] B3LYP-D3,[18] B97D3,[18] and B97D[19] under both Pople's 6-31+G(d,p) basis set and Dunning's correlation-consistent cc-pVDZ basis set.[20]

DOI: 10.1021/jacs.8b08628
J. Am. Chem. Soc. 2018, 140, 14308−14313

All optimized structures had zero imaginary frequencies. Computed free energies of dimerization were conducted by separately calculating the dimer and diradical and using a frequency calculation to convert the electronic energies to free energies. Intermolecular dimerization free energies were corrected to the solution standard state of 1 M. Because implicit solvent models have difficulties with very low dielectric solvents such as toluene (ε = 2), the solvent used for experimentally determining dimerization free energies, computations were carried out in the gas phase. Contributions to the free energy from higher-energy conformations were ignored.

CONCLUSION

In conclusion, we have investigated the intramolecular binding thermodynamics for a series of tethered dicyanomethyl diradicals and determined that these diradicals are promising building blocks for stimuli-responsive polymers and plastics, as well as dynamic covalent assemblies, possessing remarkable stability. Stronger *para* donating groups weaken the bonding interaction and lower the energy of the pimer relative to the sigma dimer. These diradical compounds have an advantage to the monoradical dimer species in that they exhibit orders of magnitude weaker binding, leading to an increase in the amount of radical at lower temperatures, in addition to having a spin−spin interaction that is concentration-independent. In all cases, temperature-responsive switching was observed, and the sensitivity can be tuned by both the attachment point and the length of the linker by changing the bonding thermodynamic parameters. Incorporation of these diradical building blocks into solid-state materials is currently being explored.

ASSOCIATED CONTENT

Supporting Information

The Supporting Information is available free of charge on the ACS Publications website at DOI: 10.1021/jacs.8b08628.

X-ray crystallographic data (CIF)
X-ray crystallographic data (CIF)
All synthetic procedures, compound characterization data, van't Hoff plots, Cartesian coordinates, and absolute energies (PDF)

AUTHOR INFORMATION

Corresponding Author

*winter@iastate.edu

ORCID

Joshua P. Peterson: 0000-0002-9897-238X
Logan J. Fischer: 0000-0003-1166-2379
Arthur H. Winter: 0000-0003-2421-5578

Author Contributions

†Rui Zhang and Joshua P. Peterson contributed equally.

Notes

The authors declare no competing financial interest.

ACKNOWLEDGMENTS

We thank the NSF CHE 1764235 and XSEDE CHE170051 for support of this work. The authors thank Dr. Sarah Cady and the ISU chemical instrument facility for assistance with variable-temperature EPR acquisition.

REFERENCES

(1) Abe, M. *Chem. Rev.* **2013**, *113*, 7011−7088. Juetten, M. J.; Buck, A. T.; Winter, A. H. *Chem. Commun.* **2015**, *51*, 5516−5519. Buck, A. T.; Paletta, J. T.; Khindurangala, S. A.; Beck, C. L.; Winter, A. H. *J. Am. Chem. Soc.* **2013**, *135*, 10594−10597. Geraskina, M. R.; Buck, A. T.; Winter, A. H. *J. Org. Chem.* **2014**, *79*, 7723−7727.

(2) Nguyen, H. V.-T.; Chen, Q.; Rajca, A.; Johnson, J. A. *ACS Cent. Sci.* **2017**, *3*, 800−811. Rajca, A.; Wang, Y.; Boska, M.; Paletta, J. T.; Olankitwanit, A.; Swanson, M. A.; Mitchell, D. G.; Eaton, S. S.; Eaton, G. R.; Rajca, S. *J. Am. Chem. Soc.* **2012**, *134*, 15724−15727. Sowers, M. A.; McCombs, J. R.; Wang, Y.; Paletta, J. T.; Morton, S. W.; Dreaden, E. C.; Boska, M. D.; Ottaviani, M. F.; Hammond, P. T.; Rajca, A.; Johnson, J. A. *Nat. Commun.* **2014**, *5*, 5460.

(3) Nishida, S.; Morita, Y.; Fukui, K.; Sato, K.; Shiomi, D.; Takui, T.; Nakasuji, K. *Angew. Chem.* **2005**, *117*, 7443−7446. Wojtecki, R. J.; Meador, M. A.; Rowan, S. J. *Nat. Mater.* **2011**, *10*, 14−27.

(4) Morita, Y.; Suzuki, S.; Sato, K.; Takui, T. *Nat. Chem.* **2011**, *3*, 197−204. Alcón, I.; Viñes, F.; Moreira, I.; Bromley, S. T. *Nat. Commun.* **2017**, *8*, 1957. Shishlov, N. M. *Russ. Chem. Rev.* **2006**, *75*, 863−884.

(5) Rajca, A. *Chem. Rev.* **1994**, *94*, 871−893. Jin, Y.; Yu, C.; Denman, R. J.; Zhang, W. *Chem. Soc. Rev.* **2013**, *42*, 6634−6654. Rowan, S. J.; Cantrill, S. J.; Cousins, G. R. L.; Sanders, J. K. M.; Stoddart, J. F. *Angew. Chem., Int. Ed.* **2002**, *41*, 898−952.

(6) Okino, K.; Hira, S.; Inoue, Y.; Sakamaki, D.; Seki, S. *Angew. Chem., Int. Ed.* **2017**, *56*, 16597−16601. Kobashi, T.; Sakamaki, D.; Seki, S. *Angew. Chem., Int. Ed.* **2016**, *55*, 8634−8638. Yuan, L.; Han, Y.; Tao, T.; Phan, H.; Chi, C. *Angew. Chem., Int. Ed.* **2018**, *57*, 1−6. Li, H.; et al. *Chem. - Eur. J.* **2017**, *23*, 13776−13783.

(7) Rajca, A.; Wongsriratanakul, J.; Rajca, S. *Science* **2001**, *294*, 1503−1505. Rajca, A.; Utamapanya, S.; Thayumanavan, S. *J. Am. Chem. Soc.* **1992**, *114*, 1884−1885. Rajca, A.; Janicki, S. *J. Org. Chem.* **1994**, *59*, 7099−7107. Rajca, A.; Utamapanya, S.; Xu, J. *J. Am. Chem. Soc.* **1991**, *113*, 9235−9241.

(8) Peterson, J. P.; Geraskina, M. R.; Zhang, R.; Winter, A. H. *J. Org. Chem.* **2017**, *82*, 6497−6501.

(9) Geraskina, M.; Dutton, A. S.; Juetten, M. J.; Wood, S. A.; Winter, A. H. *Angew. Chem.* **2017**, *129* (32), 9563−9567.

(10) Shimomura, M.; Utsugi, K.; Horikoshi, J.; Okuyama, K.; Hatozaki, O.; Oyama, N. *Langmuir* **1991**, *7*, 760−765.

(11) Frisch, G. W. T. M. J.; Schlegel, H. B.; Scuseria, G. E.; Robb, J. R. C. M. A.; Scalmani, G.; Barone, V.; Mennucci, B.; Petersson, H. N. G. A.; Caricato, M.; Li, X.; Hratchian, H. P.; Izmaylov, J. B. A. F.; Zheng, G.; Sonnenberg, J. L.; Hada, M.; Ehara, K. T. M.; Fukuda, R.; Hasegawa, J.; Ishida, M.; Nakajima, T.; Honda, O. K. Y.; Nakai, H.; Vreven, T.; Montgomery, J. A., Jr.; Peralta, F. O. J. E.; Bearpark, M.; Heyd, J. J.; Brothers, E.; Kudin, V. N. S. K. N.; Keith, T.; Kobayashi, R.; Normand, J.; Raghavachari, A. R. K.; Burant, J. C.; Iyengar, S. S.; Tomasi, J.; Cossi, N. R. M.; Millam, J. M.; Klene, M.; Knox, J. E.; Cross, J. B.; Bakken, C. A. V.; Jaramillo, J.; Gomperts, R.; Stratmann, R. E.; Yazyev, A. J. A. O.; Cammi, R.; Pomelli, C.; Ochterski, J. W.; Martin, K. M. R. L.; Zakrzewski, V. G.; Voth, G. A.; Salvador, J. J. D. P.; Dapprich, S.; Daniels, A. D.; Farkas, J. B. F. O.; Ortiz, J. V.; Cioslowski, J.; A, D. J. *Gaussian16*; Gaussian, Inc.: Wallingford, CT, 2013.

(12) (a) Becke, A. D. *Phys. Rev. A: At., Mol., Opt. Phys.* **1988**, *38*, 3098−3100. (b) Lee, C. T.; Yang, W. T.; Parr, R. G. *Phys. Rev. B: Condens. Matter Mater. Phys.* **1988**, *37*, 785−789.

(13) Becke, A. D. *J. Chem. Phys.* **1993**, *98*, 98.

(14) Perdew, J. P.; Burke, K.; Wang, Y. *Phys. Rev. B: Condens. Matter Mater. Phys.* **1996**, *54*, 16533−16539.

(15) Perdew, J. P. *Phys. Rev. B: Condens. Matter Mater. Phys.* **1986**, *33*, 8822−8824.

(16) Schmider, H. L.; Becke, A. D. *J. Chem. Phys.* **1998**, *108*, 9624−9631.

(17) Chai, J. D.; Head-Gordon, M. *Phys. Chem. Chem. Phys.* **2008**, *10*, 6615−6620.

(18) Grimme, S.; Antony, J.; Ehrlich, S.; Krieg, H. *J. Chem. Phys.* **2010**, *132*, 132.

(19) Grimme, S. *J. Comput. Chem.* **2006**, *27*, 1787−1799.

(20) Dunning, T. H. *J. Chem. Phys.* **1989**, *90*, 1007−1023.

DOI: 10.1021/jacs.8b08628
J. Am. Chem. Soc. 2018, 140, 14308−14313